Hubble Space Telescope Detection of a Quiescent Low-Mass X-Ray Binary Companion in 47 Tucanae

THE ASTROPHYSICAL JOURNAL, 564:L17–L20, 2002 January 1

HUBBLE SPACE TELESCOPE DETECTION OF A QUIESCENT LOW-MASS X-RAY BINARY COMPANION IN 47 TUCANAE[1]

PETER D. EDMONDS,[2] CRAIG O. HEINKE,[2] JONATHAN E. GRINDLAY,[2] AND RONALD L. GILLILAND[3]
Received 2001 October 15; accepted 2001 November 11; published 2001 December 10

ABSTRACT

We present the results of a search for optical counterparts to the two quiescent low-mass X-ray binaries (X5 and X7) in the globular cluster 47 Tucanae, using high-quality *Chandra* and *Hubble Space Telescope* images. A faint blue ($V = 21.7$; $U-V = 0.9$) star within 0.″03 of the eclipsing system X5 shows variability on both short and long timescales and is the counterpart of the X-ray source. The colors and variability of this object are consistent with the combination of light from an accretion disk and a red main-sequence star (possibly somewhat larger than a normal main-sequence star with similar luminosity). No evidence is found for a star showing either variability or unusual colors near the position of X7, but a probable chance superposition of a star with $V = 20.25$ limits the depth of our search.

Subject headings: binaries: general — globular clusters: individual (47 Tucanae) — techniques: photometric — X-rays: binaries

1. INTRODUCTION

It has long been thought that quiescent low-mass X-ray binaries (qLMXBs) dominate the most luminous of the dim sources in globular clusters (Hertz & Grindlay 1983; Verbunt, Elson, & van Paradijs 1984). Recent observations using *Chandra* ACIS imaging and spectroscopy have demonstrated that this is, indeed, the case. Two systems, X5 and X7, in the massive globular cluster 47 Tuc were previously suspected to be qLMXBs (Hasinger, Johnston, & Verbunt 1994; Verbunt & Hasinger 1998), but the sensitivity and resolution of *Chandra* was required to confirm this suspicion (Grindlay et al. 2001a, hereafter GHE01a; and C. O. Heinke et al. 2001a, in preparation, hereafter HGL01). One qLMXB has also been found in each of NGC 6397 (Grindlay et al. 2001b, hereafter GHE01b) and ω Cen (Rutledge et al. 2001). These four qLMXB systems all have thermal spectra that are well modeled by hydrogen atmospheres of hot neutron stars (NSs) with no power-law components required. None of them are obviously variable with the exception of X5 (HGL01), which shows deep eclipses as well as dips indicating increased neutral hydrogen (X7 shows marginal evidence for a 5.5 hr period).

The logical extension of this work is to search for optical counterparts to these sources using the potent combination of *Chandra* and the *Hubble Space Telescope*. With astrometric errors of less than 0.″1 routinely being achieved for X-ray sources, optical identifications are being reported with unprecedented frequency. These identifications include cataclysmic variables (CVs) and BY Draconis variables (GHE01a, GHE01b), millisecond pulsars (MSPs; Edmonds et al. 2001, hereafter EGH01; and Ferraro et al. 2001), and active LMXBs (Heinke et al. 2001b; White & Angelini 2001).

Searches for optical counterparts to qLMXBs have been less successful. No counterpart has been found for the NGC 6397 qLMXB (any possible companion has $M_V > 11$; GHE01b), while the ω Cen qLMXB lies outside the field of view (FOV) of current *HST* data sets, and stellar crowding will limit deep searches from the ground. Here we report the use of high-quality *Chandra* and *HST* data to search for optical counterparts to the 47 Tuc qLMXBs X5 and X7. We have discovered a faint, blue, and variable counterpart to the eclipsing X5, as reported briefly in GHE01a. This detection, combined with the well-determined period, distance, inclination, and X-ray spectrum of X5, makes this the best-constrained qLMXB known. We also report limits on the qLMXB X7. The astrometry, photometry, and time series for both of these searches are described below.

2. OBSERVATIONS AND ANALYSIS

Details of the *Chandra* data used here are given by GHE01a and HGL01. The qLMXBs X5 and X7 have 4576 and 5488 counts, respectively (over the 72 ks observation), with internal 1 σ errors of 0.″0082 and 0.″0089, respectively. To search for optical counterparts to X5 and X7, two *HST* data sets have been analyzed: the 8.3 day observations of Gilliland et al. 2000 (GO 8267: 1999 July 3–1999 July 11) and the archival data of Meylan obtained in three different epochs with ~2 yr spacings (GO 5912: 1995 October 25; GO 6467: 1997 November 3; GO 7503: 1999 October 28). The Gilliland data provide exquisite F555W (~*V*) and F814W (~*I*) time series (with some F336W (~*U* data), and the Meylan data provide F300W images in the first two epochs and F300W and F555W images in the third epoch (with limited time series information in each epoch).

2.1. *Astrometry*

Using the zero-point positional offsets between the *Chandra* and *HST* coordinate frames, the region within ~2.″0 of the nominal X5 position lies outside the FOV of the Gilliland data set but is found on the inner part (with respect to cluster center) of the WF4 chip in the Meylan data. Since no *Chandra* source in the WF4 FOV with more than 50 counts (not including X5) currently has a plausible optical counterpart, we used the PC astrometry to align the X-ray and optical coordinate frames (incurring a systematic chip-to-chip error, assumed to be 0.″05, which dominates the total error budget). After this correction, we found that only three stars are within 0.″5 of the nominal

[1] Based on observations with the NASA/ESA *Hubble Space Telescope* obtained at STScI, which is operated by Association of Universities for Research in Astronomy, Inc. under NASA contract NAS 5-26555.

[2] Harvard-Smithsonian Center for Astrophysics, 60 Garden Street, Cambridge, MA 02138; pedmonds@cfa.harvard.edu, cheinke@cfa.harvard.edu, josh@cfa.harvard.edu.

[3] Space Telescope Science Institute, 3700 San Martin Drive, Baltimore, MD 21218; gillil@stsci.edu.

X5 position, with separations of 0.″033 (0.6 σ; C1), 0.″23 (4.5 σ; C2), and 0.″292 (5.7 σ; C3). The finding chart shows the F300W and F555W images (Figs. 1*a* and 1*b*, respectively) from Meylan epoch 3 for the region around X5, and the insets in Figure 1*a* show epochs 1 and 2, U (1) and U (2), respectively. Since faint red main-sequence (MS) stars appear brighter in the F555W image than in the F300W image, Figures 1*a* and 1*b* show that C1 has a blue color. However, C3 (just outside the 5 σ error circle to the northeast) has an even stronger blue color and so is also a potentially viable optical counterpart, if the astrometric shift between the PC and WF4 chips is much larger than assumed. This ambiguity is resolved by noting that C1, unlike C3, is clearly brighter in epoch 1 than in epoch 2 (see Fig. 1*a*, *inset*) confirming it as the optical counterpart (hereafter $X5_{opt}$; see Table 1).

The region within a few arcseconds of X7 falls on the PC images of both the Gilliland and Meylan data sets. Since 17 *Chandra* sources have likely optical counterparts on the Gilliland PC image, we have corrected for small linear terms in the residual astrometric errors between *Chandra* and *HST* using least-squares fitting. We computed the positional errors for X7 by adding the systematic errors to the random WAVDETECT errors in quadrature, resulting in 1 σ errors of 0.″0065 in R.A. and 0.″0088 in decl. (see Figs. 1*c* and 1*d*, where 20 σ error circles are shown). The three nearest stars to X7 in the Gilliland *HST* image are 0.″019 (2.3 σ), 0.″12 (14.7 σ), and 0.″23 (28.6 σ) away (N1, N2, and N3, respectively). Clearly, astrometrically, only N1 ($V = 20.25$; $U-V = 1.72$; $M_V = 6.8$) is a viable candidate for the optical companion of X7. Given the FOV of the PC and the detected number of stars on the PC chip with $V < 20.25$ (6367), only 6.3×10^{-3} stars are expected within 0.″019 of N1, assuming constant density over the PC FOV.

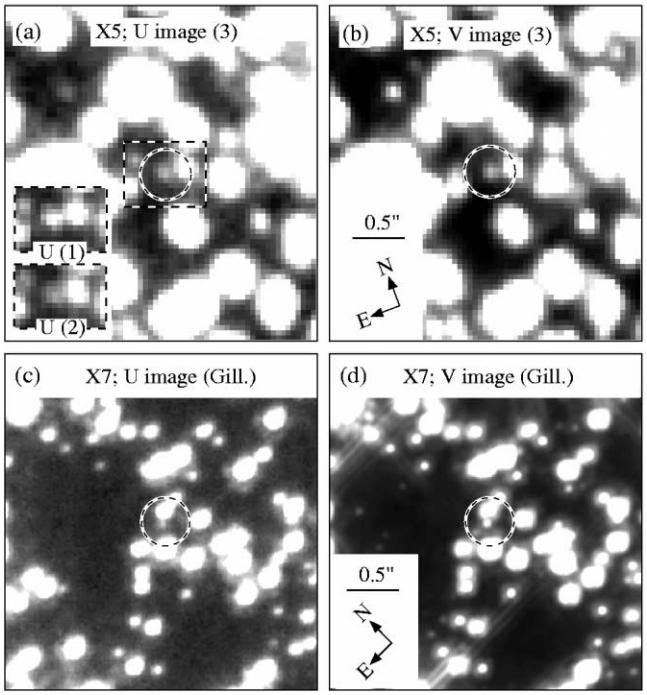

FIG. 1.—Finding charts for X5 and X7. For X5 the third-epoch combined images (*a*) F300W (*U*) and (*b*) F555W (*V*) are shown. The X5 companion ($X5_{opt}$) is near the center of the 5 σ error circle, and the inset shows the area around $X5_{opt}$ from the first and second epochs (note the clear variability of $X5_{opt}$). For X7 the deep, oversampled, combined images (*c*) F336W (*U*) and (*d*) F555W (*V*) from Gilliland et al. 2000 are shown. The star N1 is found near the center of the 20 σ error circle.

2.2. *Photometry*

The Gilliland data set photometry (containing only X7) is described in Gilliland et al. (2000) and Albrow et al. (2001). The photometry for the Meylan observations (containing X5 and X7) was based on combining the images at each epoch using drizzle routines (Hook, Pirzkal, & Fruchter 1999) in STSDAS and then using point-spread function fitting in DAOPHOT to calculate instrumental magnitudes. The F555W filter is a good approximation to Johnson *V* (Holtzman et al. 1995), but F300W differs significantly from the nearest Johnson filter (*U*). Therefore, we used ground-based photometry of 47 Tuc (Sills et al. 2000) and matching of MS turnoffs between the *HST* and ground-based data sets to calculate the zero point and then applied corrections to F300W$-V$ (by measuring MS ridgelines) to convert it to $U-V$. By definition this MS-ridgeline technique is only applied to stars (like $X5_{opt}$) with colors ranging from the MS turnoff to the detected end of the MS.

Since this technique is nonstandard, we have performed two consistency checks with other calibration methods. We applied this technique to the Meylan PC data and performed a star-by-star comparison between our photometry and the Gilliland et al. (2000) photometry. Mean differences between the two photometric systems were less than 0.05 mag in both *U* and *V*. A star-by-star comparison between the MS-ridgeline *V* calibration for the Meylan WF4 chip (containing $X5_{opt}$) and the standard calibration of Holtzman et al. (1995) applied to a 47 Tuc F555W image from the archive (program GO 6095) also gave mean errors of less than 0.05 mag. Combined with the 0.1 mag rms internal error in $U-V$ at the *U* mag of $X5_{opt}$, we estimate absolute errors for $X5_{opt}$ of ~0.2 mag in both *U* and *V*.

The color-magnitude diagrams (CMDs) for the Gilliland PC and Meylan WF4 images are shown in Figure 2. Figure 2*a* shows the mean epoch 3 CMD position of $X5_{opt}$ ($V = 21.7$; $U-V = 0.9$; $M_V = 8.2$), along with reasonable ranges in magnitude and color given the variability (see below).

TABLE 1

POSITIONAL, PHOTOMETRIC, AND TIME SERIES INFORMATION FOR X5 AND X7

qLMXB	R.A.[a] (J2000.0)	Decl.[a] (J2000.0)	X[b]	Y[b]	U[c]	V[c]	Period[d] (hr)
X5 ……	00 24 00.991(1)	−72 04 53.202(7)	60.7	263.0	22.5(2)	21.7(2)	8.67
X7 ……	00 24 03.528(1)	−72 04 51.938(6)	498.5	775.5	…	…	5.50

NOTE.—Units of right ascension are hours, minutes, and seconds, and units of declination are degrees, arcminutes, and arcseconds.

[a] Coordinates in MSP astrometric system; Freire et al. 2000.

[b] Pixel coordinates of X-ray sources using the STSDAS task METRIC applied to archival images u2ty0201t (X5) and u5jm070cr (X7).

[c] Epoch3 mean magnitudes for $X5_{opt}$.

[d] Periods from HGL01; value for X7 is from a marginal detection of variability

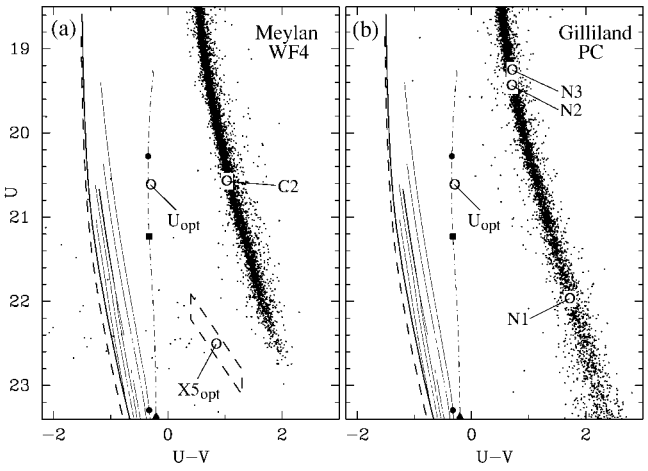

FIG. 2.—*U* vs. *U*−*V* CMDs for (*a*) the Meylan WF4 chip (containing $X5_{opt}$) and (*b*) the Gilliland PC chip (containing X7). For $X5_{opt}$ we show ranges in magnitude and color given limits on the variability. Near neighbors to $X5_{opt}$ and X7 are shown (apart from C3, which is not detected in the F555W image). Also shown are CO WD cooling sequences from Bergeron, Wesemael, & Beauchamp (1995; *thick lines*) and He WD cooling sequences from Serenelli et al. (2001; *thin lines*). The dot-dashed sequence is the lowest mass model (the MSP counterpart U_{opt} from EGH01 is also shown).

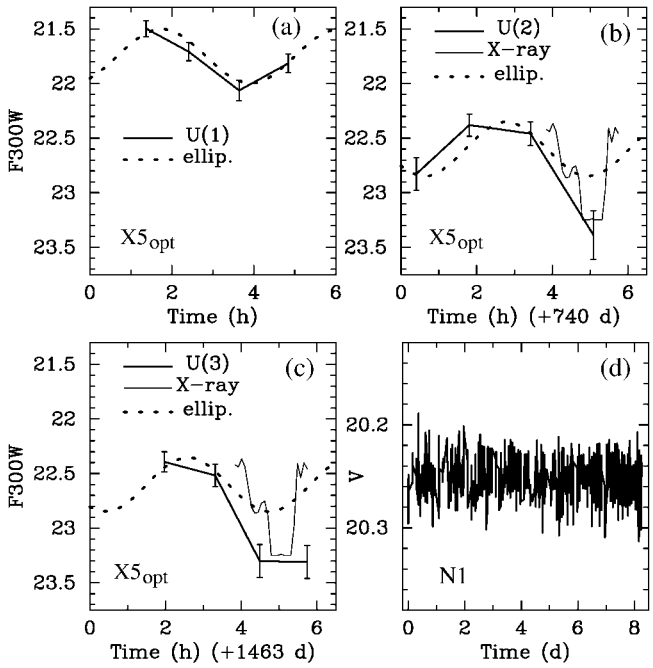

FIG. 3.—F300W time series for $X5_{opt}$ for epochs (*a*) 1, (*b*) 2, and (*c*) 3, with time offsets between epochs as shown. For $X5_{opt}$ a simple ellipsoidal model ("ellip."), eclipse not included, is shown (zero points adjusted to the data). Also shown is the eclipsed portion of the X-ray phase plot (units converted into time) from HGL01. The 1 σ error bars are the median time series rms for stars within 0.25 mag of a given magnitude level. (*d*) shows the *V*-band time series for N1, the nearest possible counterpart to X7.

With $M_V = 8.2$, $X5_{opt}$ has a similar absolute magnitude to that of the qLMXBs Cen X4 ($M_V = 7.5$–8.5; Chevalier et al. 1989) and Aql X1 ($M_V = 8.1$; Chevalier et al. 1999). Also shown are CO and He white dwarf (WD) cooling sequences (see Fig. 2 legend for details). Clearly, $X5_{opt}$ is unlikely to be either a CO WD or a He WD, unlike the MSP companion U_{opt} (EGH01). Instead, it is more likely that the CMD position of $X5_{opt}$ represents the sum of a red MS star and a blue component from an accretion disk (see below).

Figure 2*b* shows the Gilliland CMD for X7 featuring the position of the three nearest stars (N1, N2, and N3). The only astrometrically viable counterpart, N1, falls very close to the MS ridgeline (also in *V* vs. *V*−*I*) and, therefore, appears like a normal MS star (unlike $X5_{opt}$). This CMD position is consistent, within the errors, with the position in the Meylan data, and the F300W magnitudes from the three epochs are consistent with nonvariability, again unlike $X5_{opt}$. This suggests that N1 is probably not the X7 counterpart, despite the good astrometric match. Assuming that the real counterpart falls in the less confused part of a 5 σ error circle, we set limits on its detection of $U > 23$, $V > 23$, and $I > 22$ (using the Gilliland data).

2.3. *Time Series*

Since $X5_{opt}$ is near (or beyond) the limit of detectability in individual F300W exposures, the time series for $X5_{opt}$ was calculated by co-adding groups of three to four images. Figures 3*a*, 3*b*, and 3*c* show the F300W time series for the three different epochs. Also shown are the eclipsed portion of the X-ray phase plot from HGL01 (units converted into time) and a 4.333 hr period sinusoid, as appropriate for X5 but with the 8.666 hr X-ray period divided by 2 to simulate a double-peaked (ellipsoidal) time series. Eclipses are not included in this model. This model has been shifted in time and magnitude so that it plausibly matches the data for each epoch (the period is not known with sufficient accuracy to phase correct from *Chandra* to different *HST* epochs). Significant variability is seen within all three epochs, and $X5_{opt}$ is clearly brighter in epoch 1 than in epochs 2 and 3 (see Fig. 1*a*). This long-term variability is further evidence for the presence of an accretion disk. Note the deep eclipse observed in both epochs 2 and 3. The F300W eclipse appears to be significantly wider than in X-rays, though we do not observe the system coming out of eclipse. The turnover at the beginning of the second epoch (near time = 0 hr) may represent a minimum from ellipsoidal variability, since the timescale of variability agrees well with the ellipsoidal model. The first-epoch observations may also represent ellipsoidal variations rather than an eclipse, since in its brighter state the relative brightness of the disk compared to the secondary should be enhanced and the eclipse depth should increase. The *V*-band variations, not plotted here, show neither an eclipse nor clear evidence for ellipsoidal variations (expected to have a smaller amplitude than in F300W).

No suggestion of variability is present in the N1 time series (Fig. 3*d*) and no significant signal is seen in the N1 power spectrum (*V* or *I*), including the possible 5.5 hr period noted by HGL01. The highest peak in the *V* band corresponds to a period of 2.52 hr (or twice this), with a false-alarm probability of 0.27. The corresponding *V* amplitude is 0.0043 ± 0.0011 (<4 σ, insignificant for a blind search; similar results hold for *I*). If N1 *is* the X7 counterpart and is close to filling its Roche lobe, then an inclination of less than 2°.5 is required to reduce the amplitude for ellipsoidal variations from the maximum expected value of ~0.1 for a 90° inclination to less than 0.0043. This implies that N1 is unlikely to be the X7 companion, and we have calculated the brightness limit for a faint variable star (lying near the line of sight of N1) to be missed by our variability search. The X7 coordinates are so close to N1 that it will be included in any time series extraction. A star at $V = 22.9$ with intrinsic variations of 0.1 mag superposed on the time series of N1 would yield an 8 σ detection (vs. the highest

detected peak at ~4 σ). This time series limit of $V \sim 23$ for a companion to X7 will decrease for inclinations less than 90°.

3. DISCUSSION

Using the stellar models of Bergbusch & Vandenberg (1992), we estimated the brightest possible secondary consistent with our photometry ($T_{\rm eff} = 4100$ K, $V = 21.7$, and mass $= 0.53$ $M_\odot$). Using the secondary radius, the X-ray luminosity of X5, and the binary separation (from Kepler's Third Law), we estimate that the maximum luminosity from heating of the secondary by the NS (when measured as a fraction of the secondary luminosity) is 2.7%. Therefore, secondary heating probably makes only a small contribution to the variability described above. The dominant sources of short-term variability are likely to be a combination of eclipses of the disk and hot spot by the MS star, ellipsoidal variations, and flickering. Further observations are required to better define this variability.

The likely presence of an accretion disk in $X5_{\rm opt}$, from variability and the blue color, may appear to be inconsistent with the lack of X-ray evidence for accretion currently in the X5 system, which should yield either long-term X-ray variations or a power-law component, neither of which are seen (HGL01). One possible explanation is that the X5 secondary is no longer filling its Roche lobe, causing it to be detached from the disk. Such a disk would no longer be accreting matter from the secondary, possibly causing it to enter a long-term quiescent phase with low density and little or no accretion onto the NS. The X5 disk does appear to be relatively faint compared to 47 Tuc CVs, since the $U-V$ color of $X5_{\rm opt}$ (0.9) is much redder than that of the 47 Tuc CVs V1, V2, W1, and W2 with $U-V$ colors ranging from -1.25 to -0.4 (P. D. Edmonds et al. 2001, in preparation).

To test this "detached disk" theory, we have estimated the degree to which $X5_{\rm opt}$ fills its Roche lobe as defined by F, the ratio between the stellar radius and the Roche lobe radius. Using the Roche lobe formula from Paczyński (1971) ($r/a = 0.462[M_{\rm opt}/(M_{\rm NS} + M_{\rm opt})]^{1/3}$, where r is the Roche lobe radius, a is the binary separation, $M_{\rm opt}$ is the mass of $X5_{\rm opt}$, and $M_{\rm NS} = 1.4$ $M_\odot$), the stellar radius for a 4100 K model, and the binary separation, we find that $X5_{\rm opt}$ has $F = 0.6$, underfilling its Roche lobe. Fainter cooler secondaries will underfill their Roche lobes by slightly larger amounts (e.g., a star with $M_V = 10.0$ has $F = 0.5$). This behavior is consistent with the "detached disk" theory given above, but would be inconsistent with the possible detection of ellipsoidal variations of relatively large amplitude, requiring the secondary to have $F \sim 1.0$. The latter possibility would suggest that the X5 secondary is either bloated or slightly evolved, as appears to be the case for some of the CVs in NGC 6397 (J. E. Grindlay et al. 2001, in preparation), and as might be expected for a star undergoing mass loss.

If the 5.5 hr X-ray period for X7 (HGL01) is real, and if the X7 secondary underfills its Roche lobe by about the same amount as $X5_{\rm opt}$, then $M_V \sim 10.6$ and $V \sim 24.1$, beyond our variability detection limits and beyond our CMD search limit except with the presence of a reasonably bright disk. The close proximity of N1 only ~0.″02 from the line of sight of X7 clearly makes prospects for such an optical identification difficult. Alternatively, the period could be longer, and N1 could be the counterpart; however, the complete lack of evidence for a disk or variability rules against this possibility.

The logical follow-up to these observations are spectroscopic studies to measure the radial velocity amplitude of absorption lines from $X5_{\rm opt}$. This, combined with the known inclination and spectroscopic and photometric determinations of $M_{\rm opt}$ would give an estimate of the mass of the X5 NS. Using the X-ray spectrum constraints on the NS radius and redshift (HGL01) combined with the NS mass would give the first compelling test of the equation of state of a NS. Also of interest would be the detection of emission lines in the optical spectrum. Since there is evidence for an accretion disk (from this work) and hot gas in the system (from the X-ray light curve), we expect strong disk or coronal emission lines to be superposed on the absorption-line spectrum of the secondary. Study of the emission-line profiles can test for mass outflow (visible as P Cygni profiles) from the system or detect evidence for a bipolar jet (visible as broadened emission lines).

We thank Ata Sarajedini, Raja Guhathakurta, and Justin Howell for contributing to the photometric analysis and Bryan Gaensler and Frank Verbunt for comments on the manuscript. This work was supported in part by STScI grants GO-8267.01-97A (P. D. E. and R. L. G.) and HST-AR-09199.01-A (P. D. E).

REFERENCES

Albrow, M. D., Gilliland, R. L., Brown, T. M., Edmonds, P. D., Guhathakurta, P., & Sarajedini, A. 2001, ApJ, 559, 1060
Bergbusch, P. A., & Vandenberg, D. A. 1992, ApJS, 81, 163
Bergeron, P., Wesemael, F., & Beauchamp, A. 1995, PASP, 107, 1047
Chevalier, C., Ilovaisky, S. A., Leisy, P., & Patat, F. 1999, A&A, 347, L51
Chevalier, C., Ilovaisky, S. A., van Paradijs, J., Pedersen, H., & van der Klis, M. 1989, A&A, 210, 114
Edmonds, P. D., Gilliland, R. L., Heinke, C. O., Grindlay, J. E., & Camilo, F. 2001, ApJ, 557, L57 (EGH01)
Ferraro, F. R., Possenti, A., D'Amico, N., & Sabbi, E. 2001, ApJ, 561, L93
Freire, P., Camilo, F., Lorimer, D. R., Lyne, A. G., Manchester, R. N., & D'Amico, N. 2001, MNRAS, 326, 901
Gilliland, R. L., et al. 2000, ApJ, 545, L47
Grindlay, J. E., Heinke, C. O., Edmonds, P. D., & Murray, S. 2001a, Science, 292, 2290 (GHE01a)
Grindlay, J. E., Heinke, C. O., Edmonds, P. D. Murray, S., & Cool, A. M. 2001b, ApJ, 563, L53 (GHE01b)
Hasinger, G., Johnston, H. M., & Verbunt, F. 1994, A&A, 288, 466
Heinke, C. O., Edmonds, P. D., & Grindlay, J. E. 2001b, ApJ, 562, 363
Hook, R. N., Pirzkal, N., & Fruchter, A. S. 1999, in ASP Conf. Ser. 172, Astronomical Data Analysis Software and Systems VIII, ed. D. M. Mehringer, R. L. Plante, & D. A. Roberts (San Francisco: ASP), 337
Hertz, P., & Grindlay, J. E. 1983, ApJ, 275, 105
Holtzman, J. A., Burrows, C. J., Casertano, S., Hester, J. J., Trauger, J. T., Watson, A. M., & Worthey, G. 1995, PASP, 107, 1065
Paczyński, B. 1971, ARA&A, 9, 183
Rutledge, R. E., Bildsten, L., Brown, E. F., Pavlov, G. G., & Zavlin, V. E. 2001, ApJ, submitted (astro-ph/0105405)
Serenelli, A. M., Althaus, L. G., Rohrmann R. D., & Benvenuto, O. G. 2001, MNRAS, 325, 607
Sills, A., Bailyn, C. D., Edmonds, P. D., & Gilliland, R. L. 2000, ApJ, 535, 298
Verbunt, F., Elson, R., & van Paradijs, J. 1984, MNRAS, 210, 899
Verbunt, F., & Hasinger, G. 1998, A&A, 336, 895
White, N. E., & Angelini, L. 2001, ApJ, 561, L101